In: Comprehensive Guide for Nanocoatings Technology. Vol. 4 ISBN: 978-1-63482-648-8
Editor: Mahmood Aliofkhazraei

Chapter 8

NANOSTRUCTURED ANTIREFLECTION (AR) COATINGS FOR OPTOELECTRONIC APPLICATIONS

Ashok K. Sood[1], Roger E. Welser[1], Gopal G. Pethuraja[1], Adam W. Sood[1], Yash R. Puri[1], E. Fred Schubert[2], Pradeep Haldar[3], Nibir K. Dhar[4], Dennis L. Polla[5] and Priyalal Wijewarnasuriya[6]

[1]Magnolia Optical Technologies Inc., Woburn, MA
[2]Department of ECSE and Physics, Rensselaer Polytechnic Institute, Troy, NY
[3]Colleges of Nanoscale Science and Engineering
SUNY Polytechnic Institute, Albany, NY
[4]Defense Advanced Project Agency, Arlington, VA
[5]College of Science and Engineering, University of Minnesota, Minneapolis, MN
[6] Army Research Labs, Adelphi, MD

ABSTRACT

This Chapter will cover recent advances in nanostructured based detector technology i.e., materials and device for a variety of optoelectronic detection applications. The material used in this chapter will include the published work in a variety of journals and research performed under various programs in the US. The authors have many years of experience working on a variety of nanotechnologies that include a variety of semiconductors and other advanced materials for optical applications.

One of the critical technologies that will enhance the electro-optic/infrared (EO/IR) sensor performance is the development of high quality nanostructure based antireflection coating. We will discuss our results on the high performance nanostructure antireflection coatings using TiO_2 and SiO_2 graded-index nanorods deposited by oblique-angle deposition.

In this chapter, we will show that oblique angle nanowires and nanorods growth of SiO_2 and TiO_2 offer an innovative approach for developing high quality anti-refection coatings (ARC) for use on next generation sensors for both defense and commercial applications.

1. INTRODUCTION

Electro-optic/infrared (EO/IR) sensors operate in the optical radiation portion of the electromagnetic (EM) spectrum. These include Ultraviolet (UV), Visible, near-infrared (NIR) and long wave infrared (LWIR) Sensors. These sensors are being developed for use in a variety of defense and commercial applications [1–6]. Current Visible-NIR focal plane arrays (FAP) use InGaAs and SiGe that operate in 0.4 to 1.7 micron band [2].

Similarly, mid-wave infrared (MWIR) Sensors use InSb or HgCdTe based FPA's that are sensitive in 3-5 micron region [3, 4]. LWIR band uses either HgCdTe, strained-layer super lattice (SLS) structures, or Si-MEMS based Microbolometers [5, 6]. To further enhance the performance of EO/IR sensors, radiation hardened antireflection (AR) coatings have been studied in using multilayer coatings on Silicon and CdTe substrates for MWIR and LWIR applications [7].

These systems have been made possible, by substantial investment by Department of Defense (DoD) and National Aeronautics and Space Administration (NASA) in the critical technologies for short-wave infrared (SWIR), MWIR and LWIR Focal Plane Array and Sensor Packaging Technologies. These investments have provided the necessary building blocks for the infrared (IR) sensors that are being deployed in the field. These efforts have addressed the performance enhancements and producibility of the key optical components. Table 1.1 list the various semiconductors used in the EO/IR sensor and its refractive index.

The semiconductors used in EO/IR sensors have high refractive index, leading to a significant amount of reflection from the top surface. This will reduce the light throughput to the sensor and also the field of view. Hence, all of these EO/IR nanosensor technologies will benefit from the development of advanced antireflection (AR) coatings that minimize reflection losses over a wide range of wavelengths and incident angles.

Table 1.1. Refractive index of semiconductors used in EO/IR sensors

Sensor type	Semiconductors	Refractive index
Visible-NIR sensors	InGaAs, SiGe	3.71, 3.69
Mid-wave infrared sensors	InSb, HgCdTe	4.42, 3.69
Long-wave infrared sensors	HgCdTe, Si MEMS	3.69, 3.69

The use of Oblique Angle Nanowires for developing the critical technologies that will allow minimizing the reflection loss has recently been studied by Schubert et al., at RPI and reported in a paper in Nature [8]. Their work has explored the possibility of using nanowires grown by oblique angle deposition technique. Their initial investigation was based on studying the work by Lord Rayleigh that graded-refractive index layers have broadband antireflection characteristics.

Graded-index coatings with different index profiles have been investigated for broadband antireflection properties, particularly with air as the ambient medium. However, because of the unavailability of optical materials with very low refractive indices that closely match the refractive index of air, such high quality broadband antireflection coatings have not been realizable.

2. NANOWIRE ANTIREFLECTION (AR) COATING

Reducing optical reflection from surfaces is important to many applications in optics. This is commonly achieved through coating, or texturing, the surface of interest. Numerous applications involving dielectric or semiconducting materials use the light that is transmitted through the material's surface.

Examples of such application are optical lenses, windows, photovoltaic devices, and photodetectors. Glass (amorphous SiO_2) is one such dielectric material widely used in a variety of optical applications e.g., lenses, windows, and as a cover or encapsulation for semiconductor optoelectronic devices.

Glass is completely transparent for wavelengths longer than 400 nm. However, due to Fresnel reflection it reflects about 4% of the incident light from its surface (~8% from two surfaces). This reflection is undesirable in many applications as it can degrade the efficiency of the underlying device (e.g., the efficiency of a solar photovoltaic cell), reduce signal-to-noise ratio (e.g., in a photodetector), and cause glare (e.g., from LCD screens, computer monitors, and televisions).

For such applications, it is important not only to reduce reflectance but also to improve the transmittance through the surface. This requires that the coating material be non-absorbing and the coating surface be specular.

Conventionally, a single-layer coating with optical thickness equal to one quarter of the wavelength ($\lambda/4$) of interest has been used as an AR coating. Ideally such single-layer $\lambda/4$ AR coating should have a refractive index, $n_{\lambda/4}$ as given by Eq. (1) [9].

$$n_{\lambda/4} = \sqrt{n_{\text{substrate}} \times n_{\text{air}}} \,. \tag{1}$$

Often due to unavailability of materials with the desired, exact value of the refractive index, the performance of such $\lambda/4$ AR coatings deviates from the optimum. This is especially the case for low-index substrates, such as glass. An ideal single-layer $\lambda/4$ AR coating on glass surface in an air ambient would require a material with refractive index of $(1.46)^{1/2} \approx 1.2$.

There is no conventional inorganic material that has such a low refractive index. Also, fundamentally, these single-layer $\lambda/4$ AR coatings can minimize reflection only for one specific wavelength at normal incidence and they are inherently unable to exhibit spectrally broadband reduction in reflectance over wide range of angles-of-incidence.

To accomplish broadband antireflection, various antireflection mechanisms explored using wide verity of materials, process methodology and structure. Table 2.1 presents various antireflection technologies that have been developed.

In 1880, Lord Rayleigh mathematically demonstrated that graded-refractive-index layers have broadband antireflection properties. Multi-layer stacks of materials with different refractive indices have been used in order to achieve broadband reduction in reflection [10], [11]. Anti-reflection (AR) coatings with specular surface made of multiple discrete layers of non-absorbing materials can exploit thin film interference effects to reduce the reflectance while improving transmittance. Recently, it was shown that discrete multi-layer AR coatings can outperform continuously-graded AR coatings thereby offering powerful techniques to reduce reflectance [12].

Table 2.1. Various antireflection technologies

AR mechanism	AR materials	Fabrication method	Structure	Ref.
Step Graded ARC	Nanoporous SiO_2 and TiO_2 film	Oblique Angle Deposition	Nanorod arrays	[8,13] [14–16]
Graded Index ARC	Photoresist	He-Cd Laser Collimated Beams	Sinusoidal Grating Structure	[17]
Graded Index ARC	Fluropolymer, SiO_2	Soft Lithography	Hexagonal Lattice Nipple Array Structure	[18]
Moth-eye ARC	Photoresist	Krypton Laser Collimated Beams	Dimpled Surface	[19]
Moth-eye ARC	Sol-gel	Dip Coating/Holographic Exposure of photoresist/Electroforming/PVD/Replications	Periodic Subwavelength structure	[20]
Moth-eye ARC	UV curable acrylate-based resin	Nanoimprint Lithography	Pillar or cone type structure	[21]
Moth-eye ARC	AAO Membranes	Nanoimprint Lithography	Subwavelength nanorod structure	[22]
Moth-eye ARC	Perfluoropolyether and ZrO_2	Thermal Nanoimprint Lithography	Biomimetic Moth-eye nanostructures	[23]
Multilayer ARC	TiO_2/SiO_2	RF Magnetron Sputtering	Multilayer Film	[24]
Porous ARC	SiO_2 Sol Gel	Dip Coating	Porous Structure	[25]
Porous ARC	Porous SiO_2	Remote PECVD	Porous SiO_2 Film	[26]
Porous ARC	Polystyrene and PMMA, Selective Solvent (ethanol)	Spin Coating	Porous Film	[27]
Porous ARC	PMMA Latex	Spin Coating	Porous Film	[28]
Quarter-Wavelength ARC	TiO_2	Electron-Beam evaporation	Single Layer Film	[29]
Quarter-Wavelength ARC	Polystyrene	Convective Assembly	Monolayer Colloidal Film	[30]
Quarter-Wavelength ARC	SiO_2	Wet chemical Processing	Single Layer Colloidal Film	[31,32]

Optimization of multi-layer-AR coatings is a difficult challenge because of the extremely large and complex dimensional space of possible solutions. Analytical methods to optimize AR coatings are not feasible due to the complexity of the problem. Heuristic methods such as needle-optimization [33], jump-elimination [34], and genetic algorithm [35], are commonly used. Our approach utilizes a computational genetic algorithm method; the details of which were recently discussed in the literature [36].

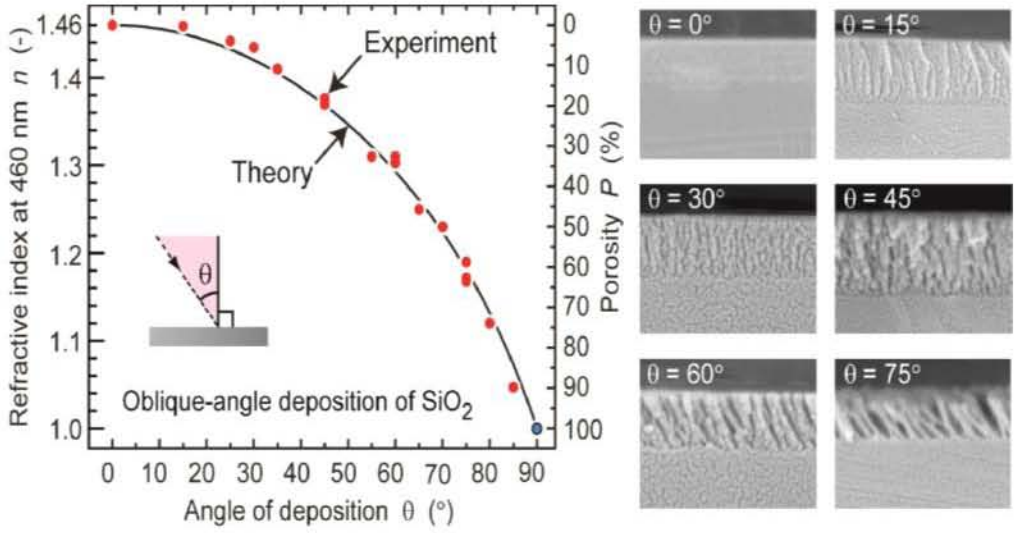

Figure 2.1. Refractive index and porosity of oblique angle deposited SiO_2 versus deposition angle. The theoretical curve is after Poxson et al. (2008) [13]. The scanning electron micrographs show a gradual increase in porosity of SiO_2 starting from a dense bulk film at 0° deposition angle and to highly nanoporous film at 75° deposition angle [37].

Until recently, due to the unavailability of optical materials with very low and tunable refractive indices ($n < 1.4$), near-perfect graded-index AR coatings could not be realized for glass substrates. We have previously demonstrated refractive index as low as 1.05 for nanoporous SiO_2 by using oblique-angle deposition [8, 38].

Figure 2.1 shows the refractive index and calculated porosity of oblique angle deposited SiO_2 versus deposition angle following the formula developed by Poxson et al., [13]. The figure shows the tunability of the refractive index of an optical material to virtually any value between its bulk value and a value close to 1.0. The scanning electron micrographs in Figure 2.1 show the gradual increase in porosity of a SiO_2 film starting from a dense bulk film deposited at an angle of 0° to a highly nanoporous film deposited at 75°.

Unlike any other method, the use of porous nano-materials fabricated by oblique-angle deposition, as described in this chapter, offers advantages such as tunability of refractive index, flexibility in choice of material, simplicity of a physical vapor deposition process, and the ability to optimize the coating for any substrate-ambient material system. For multi-layer AR coatings reported here, the refractive index of the layers is step-graded, i.e., decreased in discrete steps, from the substrate value, 1.46, to a value of 1.18.

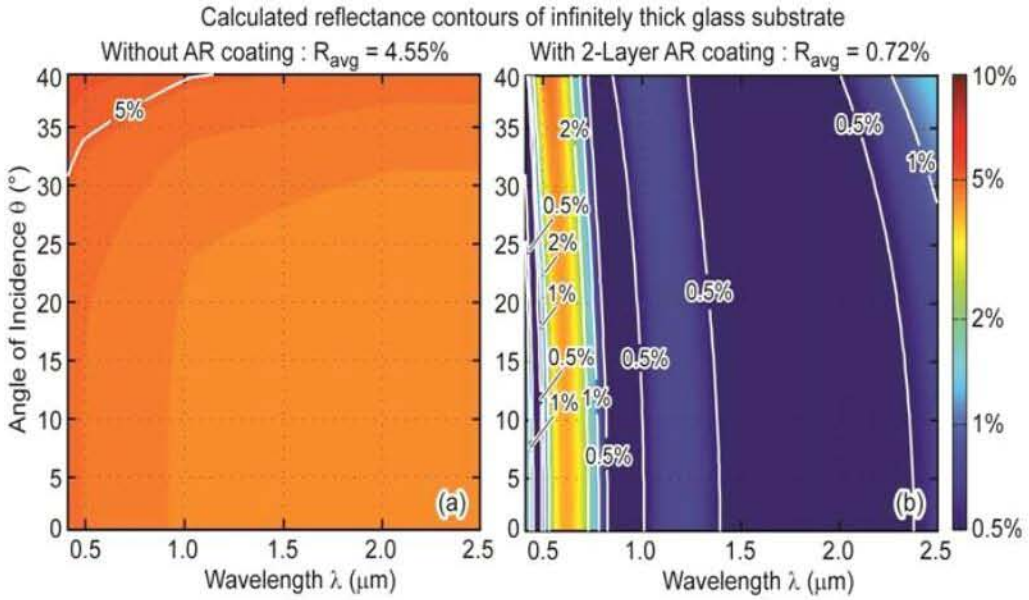

Figure 2.2. Contour plots of calculated reflectance versus wavelength and angle of incidence for an infinitely thick glass substrate with (a) no AR coating, and (b) single-side two-layer AR coating [37].

Figure 2.2 presents contour plots of the calculated reflectance as a function of wavelength and angle of incidence for a thick glass substrate with no AR coating (Figure 2.2 a) and single side 2 layer AR coating (Figure 2.2 b) respectively.

3. Modeling of Oblique Angle Nanowire AR Coating

For over a century, much of the research on broadband and omnidirectional AR coatings, motivated by Lord Rayleigh's insight, has focused on coating-design schemes that are continuously graded or that approximate continuous grading by utilizing multiple discrete layers.

A computational genetic algorithm method was employed to design optimized discrete-layer profiles that intentionally utilize optical interference effects for AR coatings [35]. The computational genetic algorithm method is an active optimization scheme for AR coatings. With this method, virtually any figure of merit can be taken into consideration. It has been shown through this method that interference coatings utilizing discrete tailored- and low-refractive index layers are able to achieve broadband and omnidirectional AR characteristics with reflectivity lower than what is possible for a continuously graded AR profile [39–41].

3.1. Numerical Approach

Calculations begin with the generation of a population of antireflection coatings with a fixed number of layers whose thicknesses and compositions are randomly generated. A layer

may be composed of either nano-porous SiO_2 or any combination of SiO_2/TiO_2, corresponding to low-*n* and co-sputtered films, respectively.

The porosity of SiO_2 is limited to 90%, corresponding to a refractive index of 1.05, which has previously been demonstrated [8]. For each member of the population, the largest thicknesses are matched to compositions with the lowest refractive index, and then sorted so that the high-index layers are adjacent to the substrate.

This increases the population near the optimum antireflection coating – which is also expected to have monotonically decreasing refractive index and increasing thickness when moving away from the substrate – and reduces the computation time.

After the population has been formed, the fitness of each member is evaluated. The fitness is determined by the reflection coefficient averaged over the wavelength range and angle range of interest, R_{ave}, which is given by,

$$R_{ave} = \frac{1}{\lambda_2 - \lambda_1} \frac{2}{\pi} \int_{\lambda_1}^{\lambda_2} \int_{0}^{\pi/2} \frac{R_{TE}(\lambda,\theta) + R_{TM}(\lambda,\theta)}{2} d\theta \, d\lambda \tag{1}$$

Where R_{TE} and R_{TM} are the transverse electric (TE) and transverse magnetic (TM) reflection coefficients. In practice, the fitness function may easily be modified to give greater weight to certain angles of incidence or to certain wavelengths to take into account the responsivity of a particular solar cell, the solar spectrum, or the orientation of a solar cell with respect to the sun, in order to maximize the power produced by a solar cell, for example.

The fittest member of the population is the one with lowest average reflection coefficient. The method for calculating the reflection coefficients of a multilayer stack was described by Born and Wolf [42]. The population is sorted by fitness, and a percentage of the worst members are then discarded.

These are replaced by the offspring of two other antireflection coatings, which are selected at random from the remaining members of the population. Offspring antireflection coatings are generated by a process of crossover and mutation. In crossover, a set of layers for the new offspring is taken from one parent, and the remainder is taken from the second parent. In mutation, the composition and thickness of each layer is given a random perturbation.

Once the worst members of the population have been replaced by new offspring, the fitness of each is evaluated, and the process repeats until good convergence is achieved. Finally, using a deterministic algorithm, the local minima near the fittest member of the population is found.

3.2. Performance and Simulation of Nanowire AR Coating

The design of optimized AR coatings for several substrates were investigated (Si, SiGe, GaN, CdTe) by using the genetic algorithm. The algorithm calculations were carried out in order to optimize AR coatings on Si, SiGe, GaN, and CdTe substrates. In the calculation, experimentally acquired refractive index values are used.

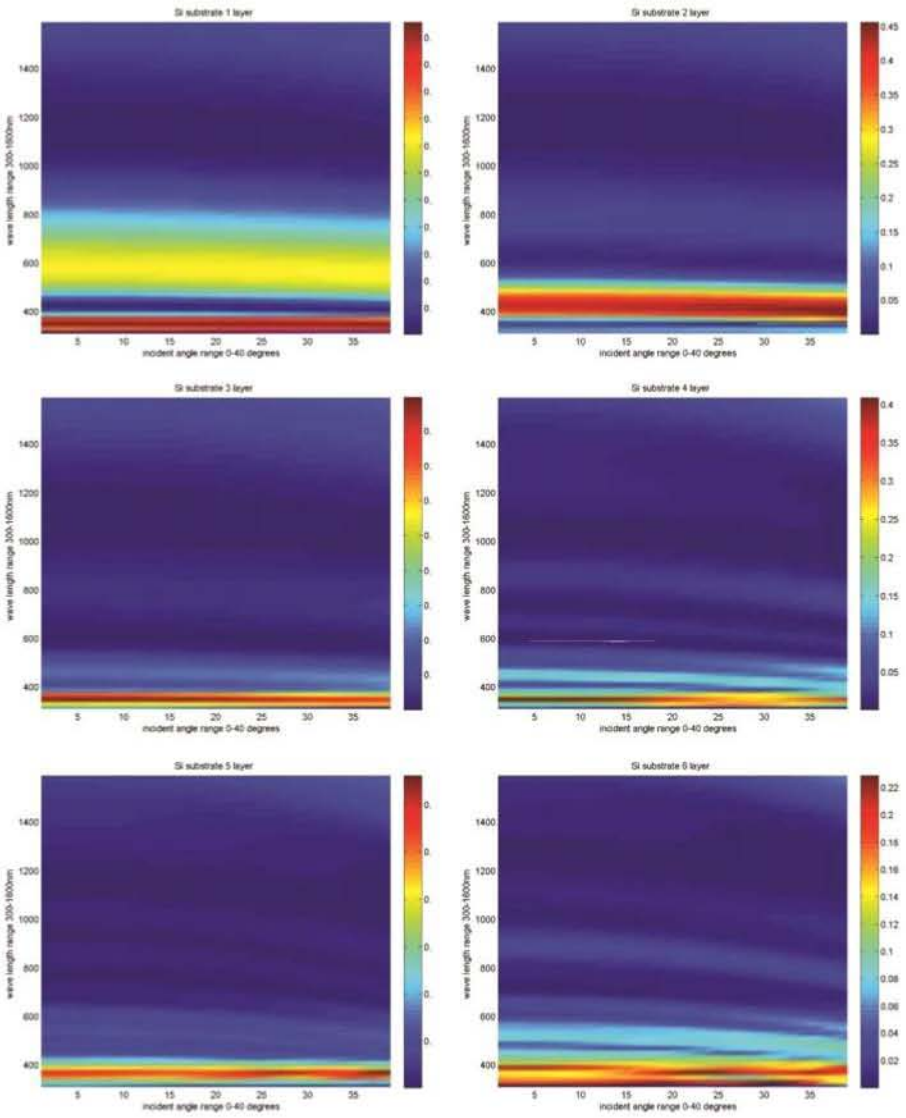

Figure 3.1. Calculated reflectivity of AR coatings, optimized for 1 ~ 6 layers each; 0 ~ 40 degree angle of incidence; 0.3~1.6 micron spectral range, on Si substrate as functions of angle of incidence and wavelength [35].

Figure of merit of this calculation is average reflectivity under following conditions:

- Angle of incidence: 0 ~ 40 degree
- Spectral range: 0.3~1.6 μm for Si wafer
- 0.3~2.5 μm for SiGe wafers
- 0.4~2.5 μm for GaN and CdTe wafer

Figure 3.1 presents calculated reflectivity of AR coatings as a function of angle of incidence and wavelength for silicon wafer. The spectral range used for this analysis ranges from 0.3 to 1.6 microns. Figure 3.2 presents calculated reflectivity of AR coatings, optimized

for 1 ~ 6 layers each; 0 ~ 40 degree angle of incidence; 0.3-2.5 micron spectral range, on SiGe substrate as functions of angle of incidence and wavelength.

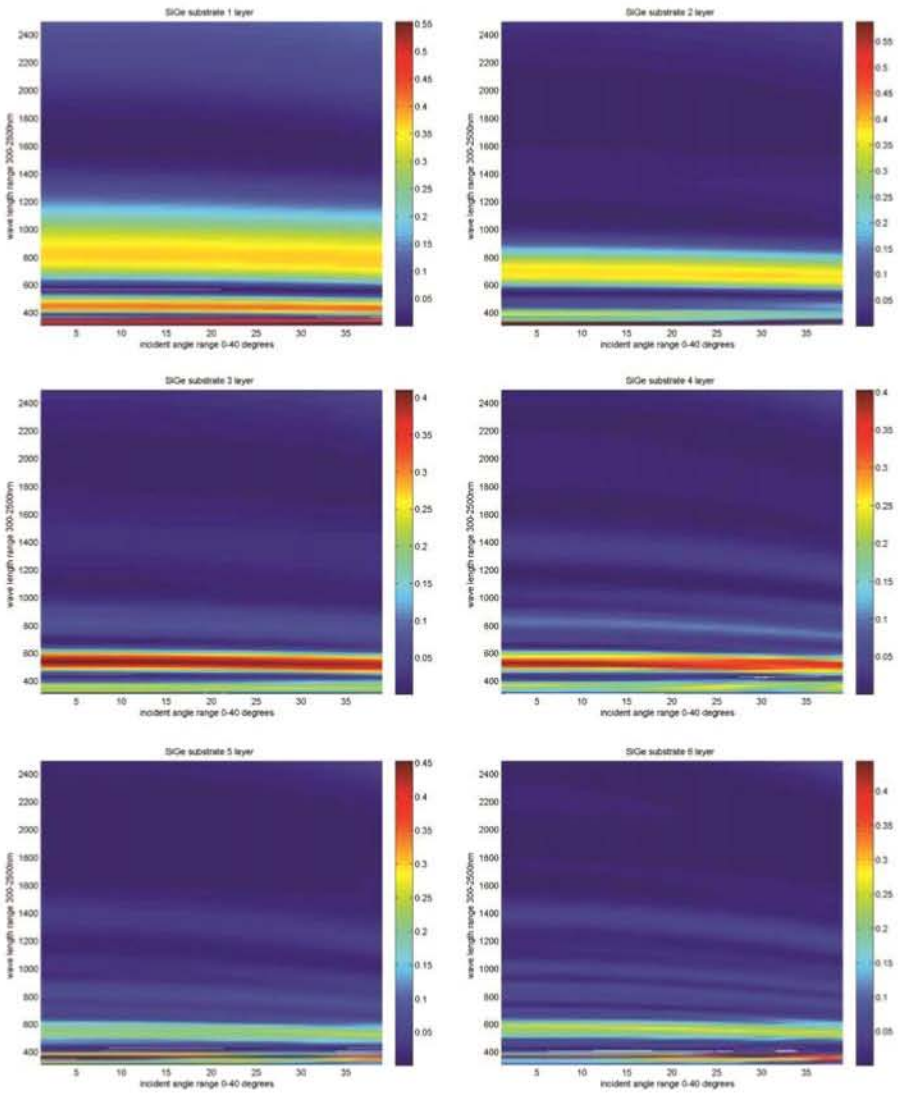

Figure 3.2. Calculated reflectivity of AR coatings, optimized for 1 ~ 6 layers each; 0 ~ 40 degree angle of incidence; 0.3-2.5 micron spectral range, on SiGe substrate as functions of angle of incidence and wavelength [35].

Figure 3.3 shows calculated reflectivity of AR coatings, optimized for 1 ~ 6 layers each; 0 ~ 40 degree angle of incidence; 0.4-2.5 micron spectral range, on GaN substrate as functions of angle of incidence and wavelength.

Figure 3.4 Calculated reflectivity of AR coatings, optimized for 1 ~ 6 layers each; 0 ~ 40 degree angle of incidence; 0.4-2.5 micron spectral range, on CdTe substrate as functions of angle of incidence and wavelength.

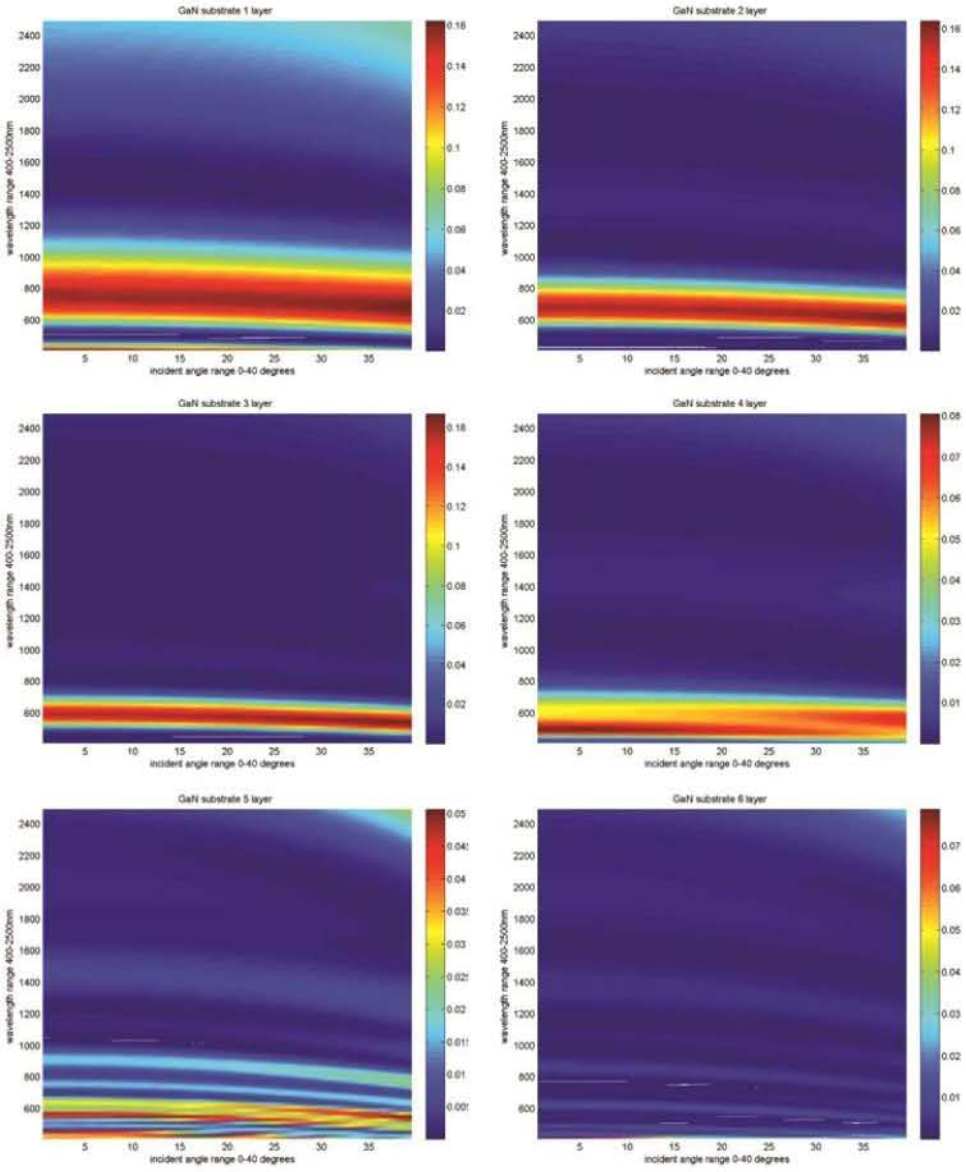

Figure 3.3. Calculated reflectivity of AR coatings, optimized for 1 ~ 6 layers each; 0 ~ 40 degree angle of incidence; 0.4-2.5 micron spectral range, on GaN substrate as functions of angle of incidence and wavelength [35].

Figure 3.5 summarizes the calculated average reflectivity as a function of number of layers on Si, SiGe, GaN and CdTe substrates. This analysis shows that high quality AR coatings can be modeled.

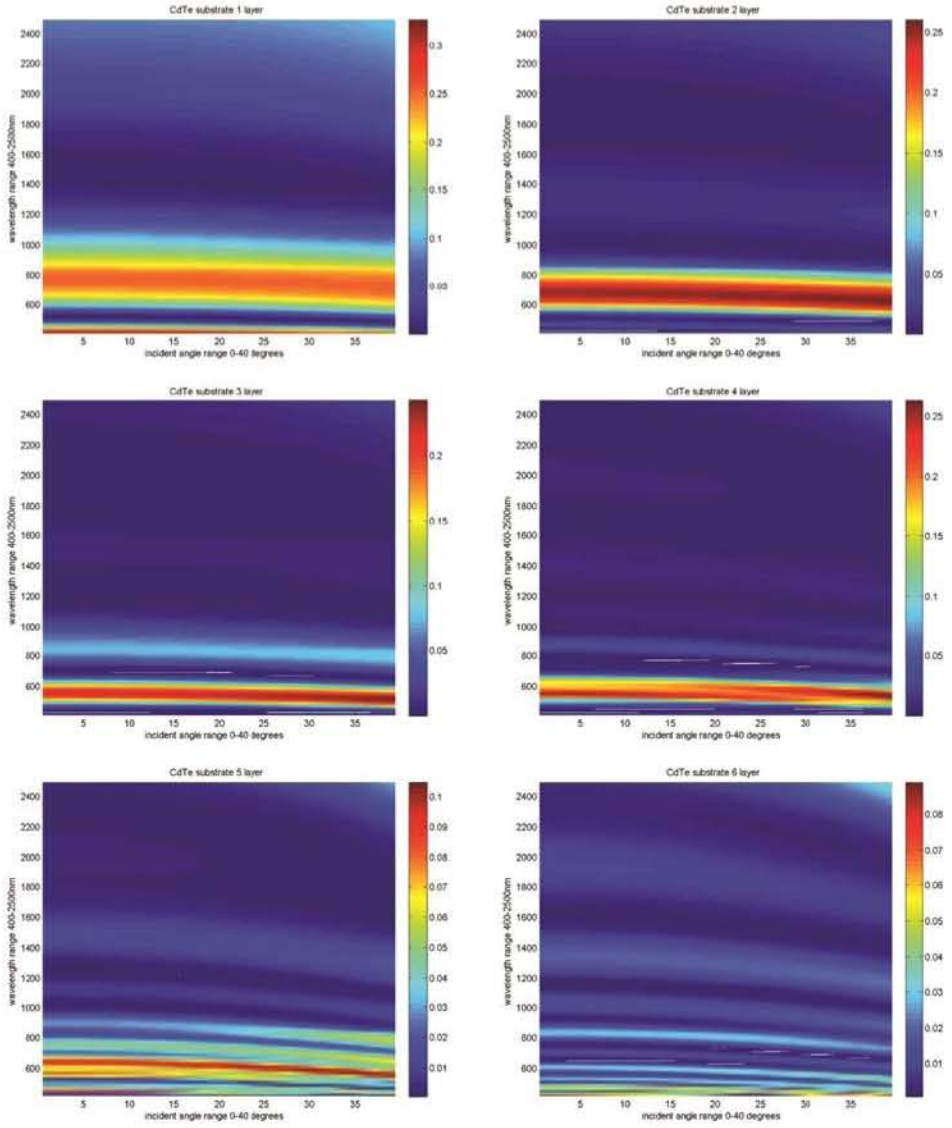

Figure 3.4. Calculated reflectivity of AR coatings, optimized for 1 ~ 6 layers each; 0 ~ 40 degree angle of incidence; 0.4-2.5 micron spectral range, on CdTe substrate as functions of angle of incidence and wavelength [35].

4. Design Optimization

Optimization of multilayer antireflection coatings is difficult because of the high cost of evaluating the performance for a given structure. In addition, the parameter space generally includes many local minima, which makes deterministic optimization schemes that find the local minima unsuitable. To meet these challenges, genetic algorithms have previously been applied in order to optimize a variety of optical coatings. Genetic algorithms mirror biological

evolution in which the fitness of a population is increased by the processes of selection, crossover, and mutation.

In this work, we apply a genetic algorithm to optimize antireflection coatings for silicon image sensors, silicon solar cells, and triple-junction Ge/GaAs/GaInP solar cells with air as the ambient medium. The calculations consider coatings composed of co-sputtered and low-n materials and take material dispersion into account.

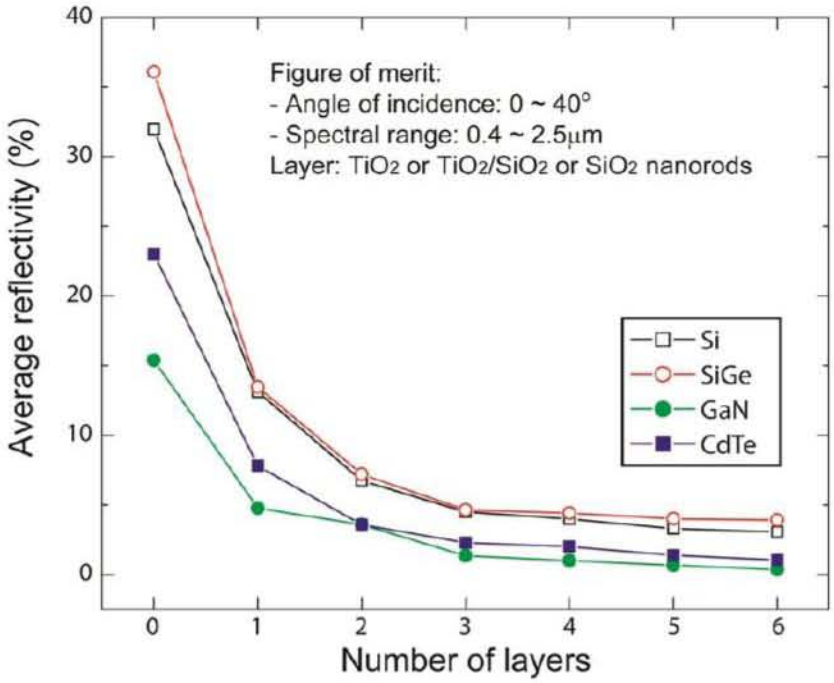

Figure 3.5. Calculated average reflectivity as a function of number of layers on Si, SiGe, GaN and CdTe substrates [35].

4.1. Silicon Image Sensor

Silicon image sensors are widespread in defense and commercial applications, and generally capture light in the visible wavelength range. Low reflection from the sensor surface is desirable to increase the absorbed light and decrease the noise in the resultant image. The reflection coefficient should also be low over a wide range of incident angles; depending upon lens configuration, the angle of incidence of light on the sensor surface can vary. Strong angular dependence of reflection can produce undesirable vignetting. Finally, the reflection coefficient must be consistently low across the entire visible wavelength range of 400 to 700 nm.

Figure 4.1 shows the reflection coefficient of bare silicon and optimized one- and three-layer antireflection coatings as a function of wavelength and incident angle. The reflection for bare silicon is high throughout the range of wavelengths and angles.

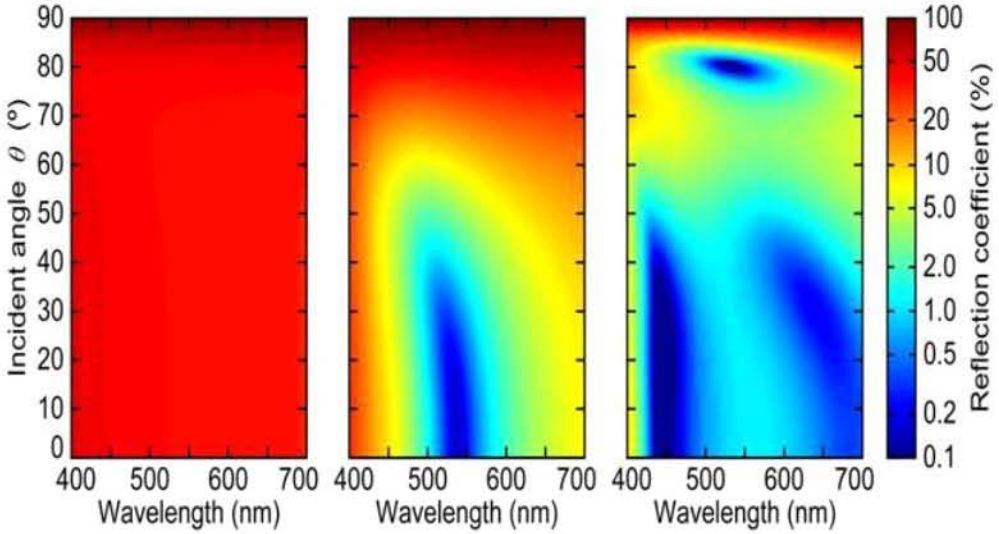

Figure 4.1. Reflection coefficient of (left) silicon and optimized (center) one- and (right) three-layer antireflection coatings for silicon image sensors versus wavelength and incident angle [35].

The single-layer coating has a minimum near λ = 540 nm at small angles of incidence, where the reflection coefficient is below 0.5%, and reduced reflection coefficient values throughout the range compared to bare silicon. The three-layer coating has three distinct minima which combine to give reflection coefficients less than 2% for the majority of wavelengths and incident angles; for optimized antireflection coatings for the silicon image sensor, the number of local minima in reflection is equal to the number of layers used. The layer compositions and thicknesses of these optimized coatings are listed in Table 4.1.

Table 4.1. Thickness *t* (in nm) and composition *c* of individual layers for optimized silicon image sensor antireflection coatings. (CS = co-sputtered layer, NP = nano-porous low-*n* layer)

	1-layer	2-layer	3-layer	4-layer
t_1	68.4	327.7	362.8	293.4
t_2	-	65.6	91.9	115.6
t_3	-	-	42.7	75.4
t_4	-	-	-	41.7
c_1	CS, 36% TiO_2	NP, 14% SiO_2	NP, 10% SiO_2	NP, 10% SiO_2
c_2	-	CS, 42% TiO_2	CS, 4% TiO_2	NP, 35% SiO_2
c_3	-	-	CS, 98% TiO_2	CS, 15% TiO_2
c_4	-	-	-	CS, 100% TiO_2

Layer thicknesses and compositions should be within several percent of the specified values in order to achieve performance similar to the given structure. In the optimized antireflection structures for the silicon image sensor, generally about half of the layers are composed of nano-porous low-*n* SiO_2. The same is true for antireflection coatings optimized for other applications, as will be shown later. This finding underscores the importance of low-*n* materials in achieving high performance antireflection coatings.

The reflection coefficient as a function of layer number for optimized coatings is shown in Figure 4.2. The reflection coefficient initially decreases rapidly as more layers are added, and then becomes almost constant.

The angle- and wavelength-averaged reflectivity of the three- and four-layer antireflection coatings are similar at 4.4% and 3.9%, respectively; the top layers of the three- and four-layer antireflection coatings each are composed of 90% porous SiO_2 – which gives the lowest allowed refractive index, while the bottom layers of both coatings are pure or nearly-pure TiO_2 – which gives the highest achievable refractive index.

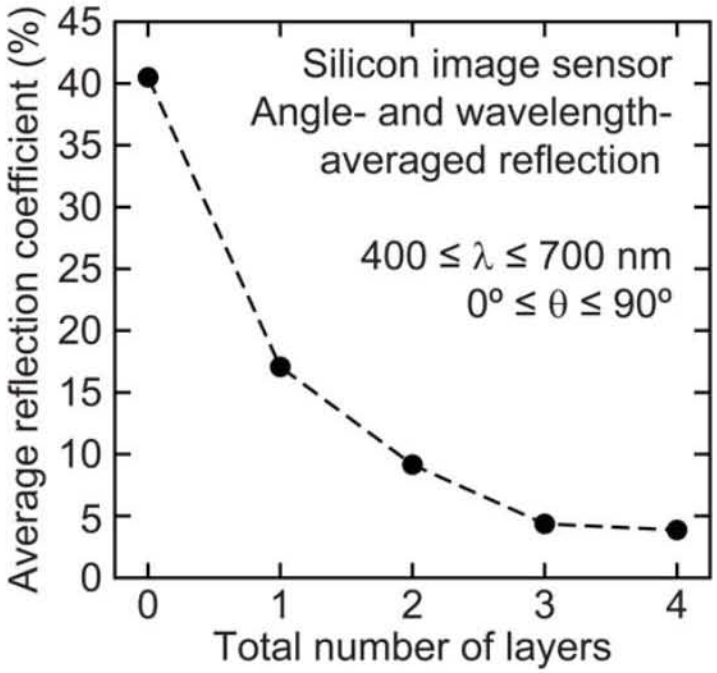

Figure 4.2. Angle- and wavelength-averaged reflection coefficient as a function of the number of layers for optimized antireflection coatings for a silicon image sensor [35].

As mentioned above, the three- and four-layer coatings also have similar reflection coefficients. This is a general characteristic for antireflection coatings: once a sufficient number of layers is used so that the optimum stack contains layers with both the highest and lowest allowed refractive index, increasing the layer number further has only a small effect on the reflection coefficient.

4.2. Silicon Solar Cell

The silicon solar cell is one of the most widespread technologies for photovoltaics; the relevant spectral range for this application is 400 to 1100 nm. One or two-layer antireflection coatings and surface texturing are common methods used to reduce reflection from the surface and increase efficiency. Using the genetic algorithm approach, antireflection coatings for silicon solar cells with up to five layers are optimized.

The reflection coefficient as a function of wavelength and incident angle is shown in Figure 4-3 for optimized one-, two-, and four-layer antireflection coatings. As before, the number of minima in reflection is equal to the number of layers in the antireflection coating. The compositions of optimized coatings are shown in Table 4-2. Again, nano-porous layers compose roughly half of the layers in an antireflection coating with a given number of layers.

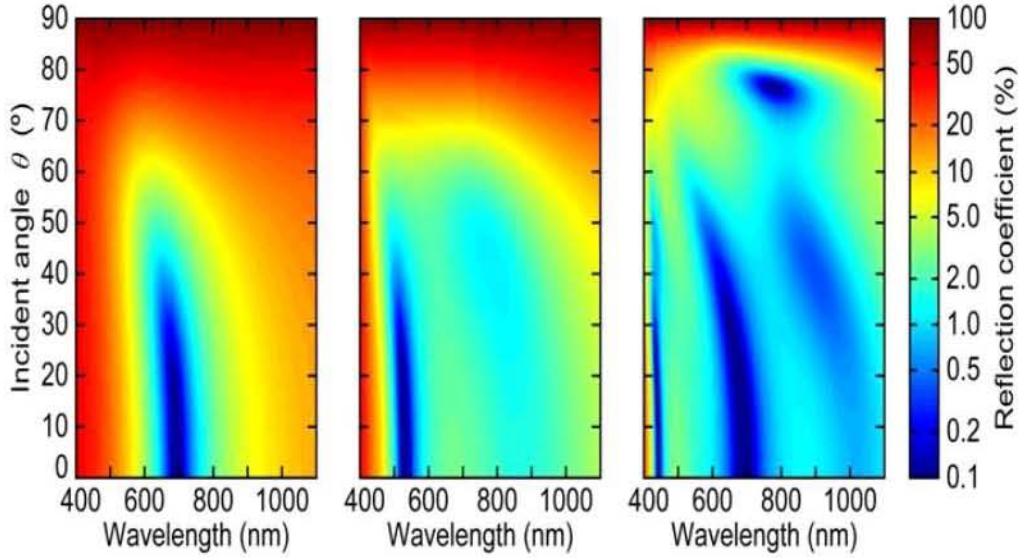

Figure 4.3. Reflection coefficient of (left) one-, (center) two-, and (right) four-layer antireflection coatings optimized for silicon solar cells versus wavelength and incident angle [35].

Compared to the one- and two-layer coatings, the four-layer coating yields substantially reduced reflection, particularly at the largest incident angles and shortest wavelengths. Note that the one- and two-layer coatings feature one co-sputtered layer and both nano-porous low-n and co-sputtered layers, respectively, which will give enhanced performance compared to conventional one- and two-layer coatings. The angle- and wavelength-averaged reflection.

Coefficients are plotted in Figure 4.4 as a function of the number of layers. As discussed above, when an optimized antireflection coating includes layers with both the lowest allowed and highest allowed refractive index, adding additional layers generally provides little benefit.

In the case of the silicon solar cell, which is identical to the image sensor with the exception that the relevant wavelength range is broader, a larger number of layers is needed to reach this threshold.

Table 4.2. Thickness t (in nm) and composition c of individual layers for optimized silicon solar cell antireflection coatings (CS = co-sputtered layer, NP = nano-porous low-n layer)

	1-layer	2-layer	3-layer	4-layer	5-layer
t_1	91.2	133.1	432.8	432.6	388.7
t_2	-	64.0	113.3	145.8	159.3
t_3	-	-	58.6	79.7	107.8
t_4	-	-	-	51.2	70.1
t_5	-	-	-	-	50.5
c_1	CS, 36% TiO_2	NP, 78% SiO_2	NP, 11% SiO_2	NP, 10% SiO_2	NP, 10% SiO_2
c_2	-	CS, 70% TiO_2	CS, 3% TiO_2	NP, 54% SiO_2	NP, 29% SiO_2
c_3	-	-	CS, 82% TiO_2	CS, 28% TiO_2	NP, 81% SiO_2
c_4	-	-	-	CS, 100% TiO_2	CS, 37% TiO_2
c_5	-	-	-	-	CS, 100% TiO_2

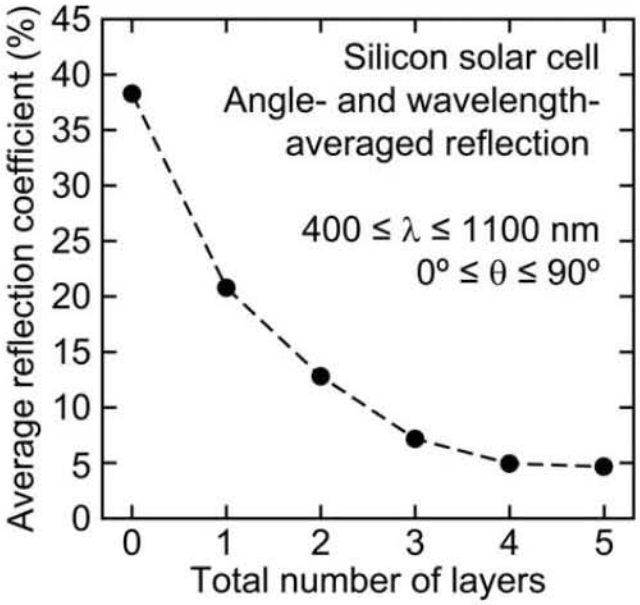

Figure 4.4. Angle- and wavelength-averaged reflection coefficient as a function of the number of layers for optimized antireflection coatings for silicon solar cells [35].

In the image sensor, going from three to four layers reduces average reflectivity by 11.1%, while for the solar cell, reflectivity is reduced by 31.1%. Adding an fifth layer to the solar cell antireflection coating reduces reflection by an additional 5.6%.

We have described a method for optimizing antireflection coatings made of co-sputtered and nano-porous low-refractive-index coatings. The method is based on a genetic algorithm which is well suited for the task of optimizing optical thin-film coatings, given the fact that the design space of multi-layered optical coatings includes many local minima of the fitness

function, i.e., the average reflectivity. The optimization method was applied to silicon image sensors and solar cells. In each case, nano-porous layers constitute roughly half of the total number of layers in optimized antireflection coatings, which underscores the importance of low-refractive-index materials for high-performance antireflection coatings.

5. Growth and Characterization of Oblique Angle Nanowires

The use of Nanowires for developing the critical technologies that will allow minimizing the reflection loss has recently been studied by Schubert et al., at RPI [8]. Their work has explored the possibility of using nanowires grown by oblique angle deposition technique as shown in Figure 5.1. Their investigation was based on studying the work by Lord Rayleigh that graded-refractive index layers have broadband antireflection characteristics [8].

Graded-index coatings with different index profiles have been investigated for broadband antireflection properties, particularly with air as the ambient medium. However, because of the unavailability of optical materials with very low refractive indices that closely match the refractive index of air, such high quality broadband antireflection coatings have not been realizable. The work carried out by Schubert et al., [8] uses TiO_2 and SiO_2 graded-index nanowires and nanorods deposited by oblique-angle deposition, and, for the first time, demonstrated their potential for antireflection coatings by virtually eliminating Fresnel reflection from an AlN–air interface over the UV band. This was achieved by controlling the refractive index of the TiO_2 and SiO_2 nanorod layers, down to a minimum value of n = 1.05, the lowest value so far reported [8].

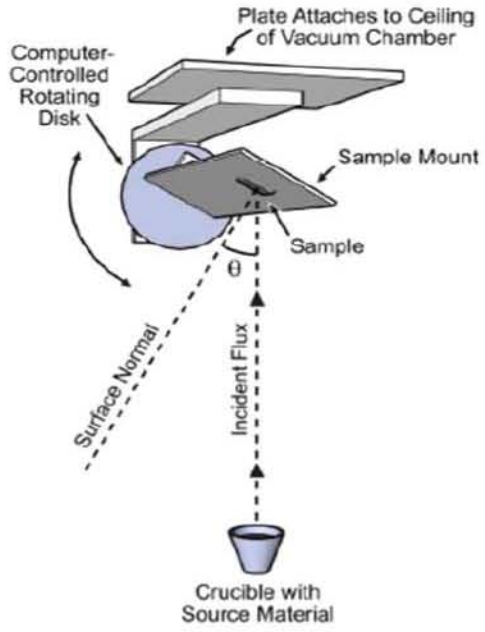

Figure 5.1. Oblique angle deposition technique for growth of nanowires/ nanorods based Anti - Reflection Coatings by E-beam evaporation [38, 43].

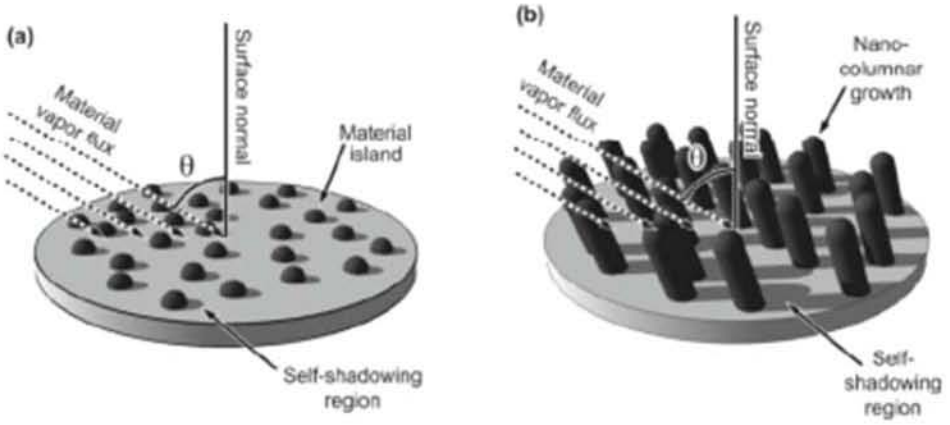

Figure 5.2. (a) Oblique angle deposition technique for growth initiation of Nanowires and Nanorods showing the vapor flux and the self-shadowed region. (b) Growth of oblique angle nanowires as a function of vapor flux [38, 43].

Figure 5.1 presents the detailed layout of the Oblique angle deposition technique for growth of oblique angle nanowires by e-beam evaporation. This technique allows for highly directional vapor flux and can be implemented with a variety of materials needed for growth of oblique angle nanowires.

Figure 5.2 presents the Oblique angle deposition technique for growth initiation of Nanowires and Nanorods showing the vapor flux and the self-shadowed region. Similarly the Figure 5.2 also presents the pictorial view of non-columnar growth of oblique angle nanowires as a function of vapor flux. Figure 5.3 presents the low index nanorods grown on Silicon substrate using the oblique angle growth techniques using SiO_2.

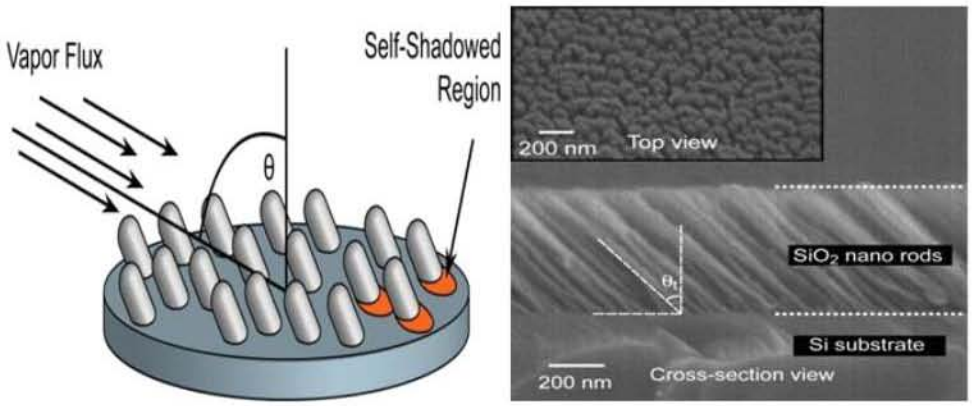

Figure 5.3. (a) Oblique angle deposition technique for growth of Nanowires/ Nanorods based anti - reflection coatings using a variety of materials i.e. SiO_2 and TiO_2 .(b) Low index SiO_2 nanorods grown on Silicon substrate showing the oblique angle of 45 degrees [44].

Figure 5.4 presents the refractive index dispersion as a function of wavelength. Measurement shown in Figure 5.4 provide dispersion curve of low index SiO_2 nanowire and nanorods thin film on silicon substrate as measured by Ellipsometry. Also shown is the comparison of experiment data with calculations. These results show, that nanowires and

nanorods grown by oblique angle techniques provides a path for broad band high quality anti-reflection coating for variety of Nanosensor Applications.

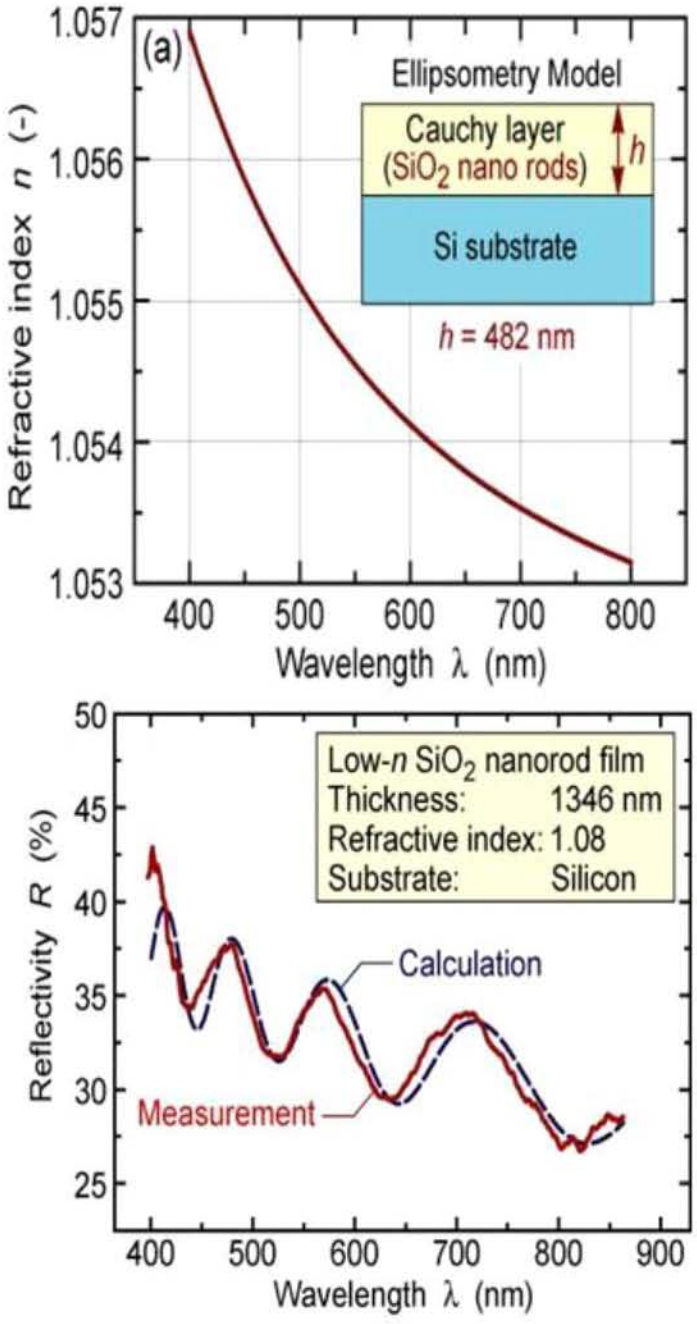

Figure 5.4. (a) Measurement of dispersion curve of low index SiO_2 nanorod thin film on Silicon substrate as measured by Ellipsometry, (b) comparison of experimental data with calculations [8].

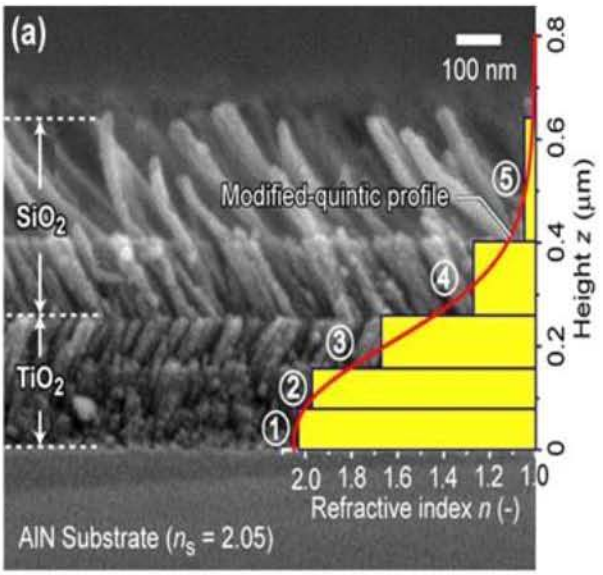

Layer No.	1	2	3	4	5
Source	TiO_2			SiO_2	
Deposition angle	25°	40°	65°	–68°	–87°
Thickness (nm)	77.4	80.2	99.3	145.0	223.0
Refractive index, *n*	2.03	1.97	1.67	1.27	1.05

Figure 5.5. (a) Demonstration of TiO_2 and SiO_2 graded index nanowire/nanorod coating with a modified-quintic profile. The graded-index coating consists of three TiO_2 nanorod layers and two SiO_2 nanorods layers. (b) The source material for each layer with deposition angle, thickness and refractive index [8].

Figure 5.5 shows the use of SiO_2 and TiO_2 nanowire and nanorods to demonstrate high quality anti-reflection coating on AlN substrate. The feasibility of this technology has been demonstrated for UV LED applications [8]. Our goal is to develop this technology for UV and other bands of interest in the NIR, SWIR and MWIR bands for next generation EO/IR Sensors.

Figure 5.6 presents reflectivity of graded-index coating on AlN substrate with a schematic of reflectivity measurement. Also shown in Figure 5.6 b is theoretical (solid line) and measured (dotted line) reflectivity versus incident angle of graded-index coating. Figure 5.6c presents wavelength dependence of theoretical (solid line) and measured (dashed line) reflectivity of graded-index coating at normal incidence [8].

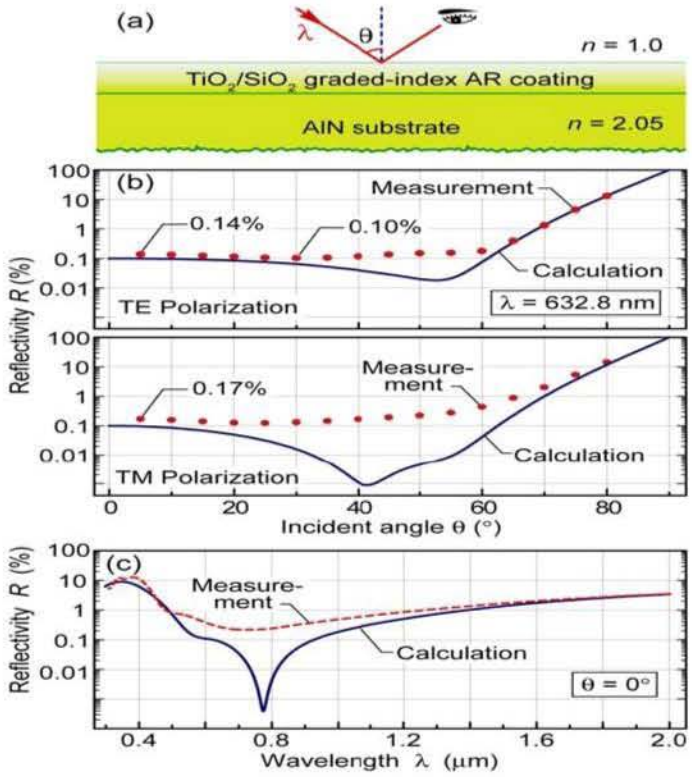

Figure 5.6. Reflectivity of graded-index coating on AlN substrate (a) Schematic of reflectivity measurement. (b) Theoretical (solid line) and measured (dotted line) reflectivity versus incident angle of graded-index coating, (c) Wavelength dependence of theoretical (solid line) and measured (dashed line) reflectivity of graded-index coating at normal incidence [8].

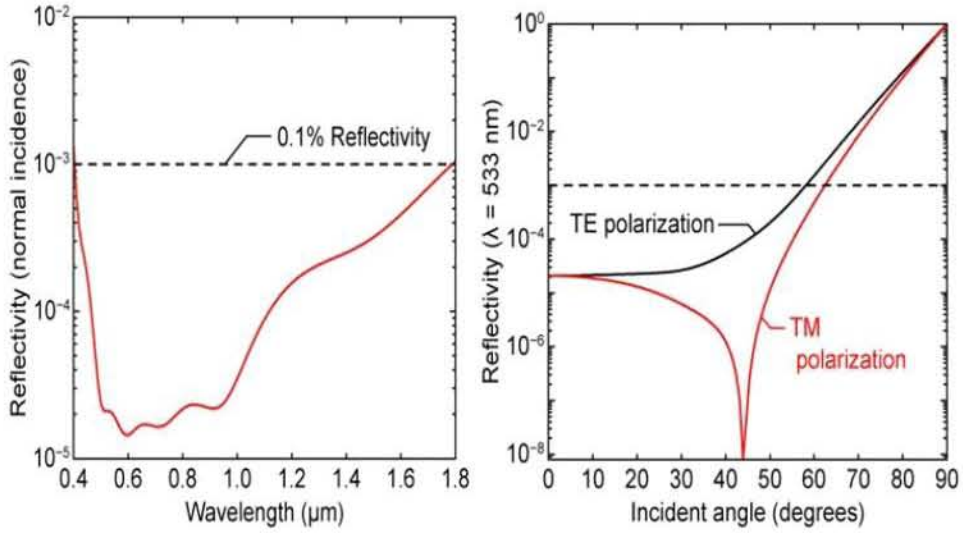

Figure 5.7. (a) Simulation of reflectivity as a function of wavelength for Visible-NIR from 0.4 to 1.8 microns using oblique angle nanowires, (b) Simulation of reflectivity as a function of polarization for incident angles from 0 to 90 degrees [38].

Figure 5.7(a) presents the simulation of reflectivity as a function of wavelength from Visible to Near Infrared band; from 0.4 to 1.8 microns using oblique angle nanowires.

Figure 5.7 (b) demonstrates the simulation of reflectivity as a function of polarization for incident angles from 0 to 90 degrees. The results show that modeling and simulation can be used effectively for developing nanowire based high quality antireflection coating that provides coverage form UV, Visible and to NIR bands.

5.1. Experimental Results

In this section, we describe our AR coating design as a two-layer AR coating with each layer having a tailored refractive index fabricated by using oblique angle electron-beam deposition. The appropriate deposition angle was then chosen for the deposition of the actual AR coating layers based on Figure 5-8 and the required value of the refractive index [37]. Three samples were prepared: (a) a reference glass substrate with no AR coating (called Sample A), (b) a glass substrate with two-layer AR coating on one side (called Sample B), and (c) a glass substrate with two-layer AR coating on both sides (called Sample C).

The two-layer AR coating is composed of a 1st layer of porous SiO_2 (P = 22%, n = 1.36 at 630 nm, t = 197 nm) deposited at 54° substrate angle, and a 2nd layer of porous SiO_2 (P = 60%, n = 1.18 at 630 nm, t = 289 nm) deposited at 78° substrate angle.

The thickness and refractive index values of each coating are measured using variable angle spectroscopic ellipsometry. The thickness values were also confirmed using scanning electron microscopy. Note that all layers of the multi-layer AR coating are made of single material, porous silica (porous SiO_2). Silica is an excellent choice as material for AR coating on glass substrate as it is native, stable, and robust.

The optical transmittance of the multi-layer AR samples was measured using (i) a normal incidence broadband spectrophotometer measurement setup and (ii) a variable angle and wavelength dependent transmittance measurement setup.

The thickness of the glass substrate used is 250 μm, much greater than the range of wavelengths under consideration; therefore we do not expect optical interference effects from the substrate. Figure 5.8 shows the measured wavelength dependent transmittance of glass substrate with (a) no AR coating (Sample A), (b) single-side two-layer AR coating (Sample B), and (c) double-side two-layer AR coating (Sample C). The inset shows the scanning electron micrograph of the two-layer AR coating.

The wavelength dependent normal incidence transmittance of Sample A, B, and C is measured between 200 nm and 2000 nm using JASCO V-570 spectrophotometer. The measurements reveal that the average transmittance between 400 nm and 2000 nm for uncoated glass substrate is 92.2% (Sample A) and it increases to 95.1% for glass substrate with two-layer AR coating on one side (Sample B) and further increases to 98.1% for glass substrate with two-layer AR coating on both sides (Sample C). The local minima seen in the transmittance curves around 700 nm are due to the thin-film interference effects of the AR coating. The average transmittance between 1000 nm and 2000 nm for glass substrate with double side AR coating is measured to be 99.3%.

Angle dependent reflectance measurements between 350 nm and 1700 nm are performed using a custom-built laboratory setup. For each sample, the reflectance data is measured for

angles of incidence ranging between 0° and 80° with 5° increments. Figure 5.9 shows the plots of the measured angle dependent transmittance.

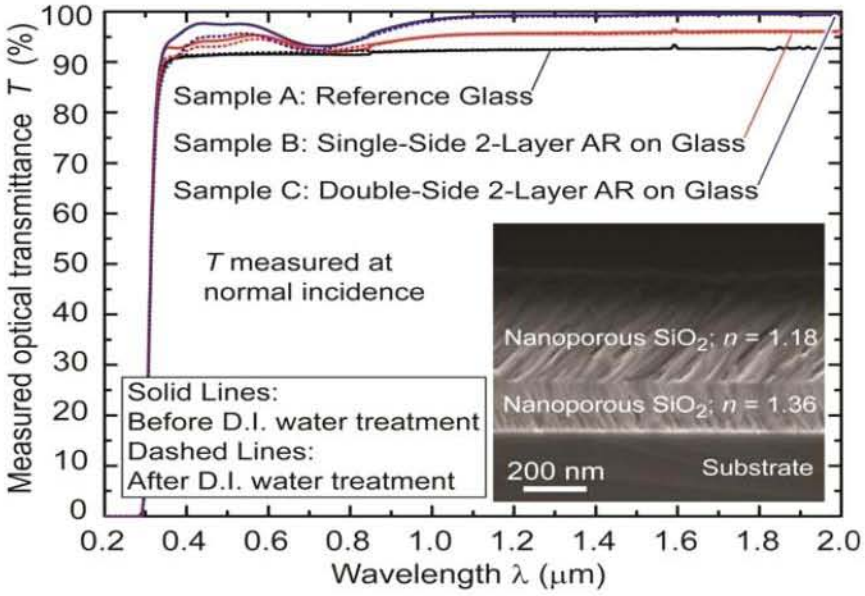

Figure 5.8. Measured wavelength dependent normal incidence transmittance of glass substrate with (a) no AR coating, (b) single-side two-layer AR coating, and (c) double-side two-layer AR coating. The inset shows the scanning electron micrograph of the two-layer AR coating [37].

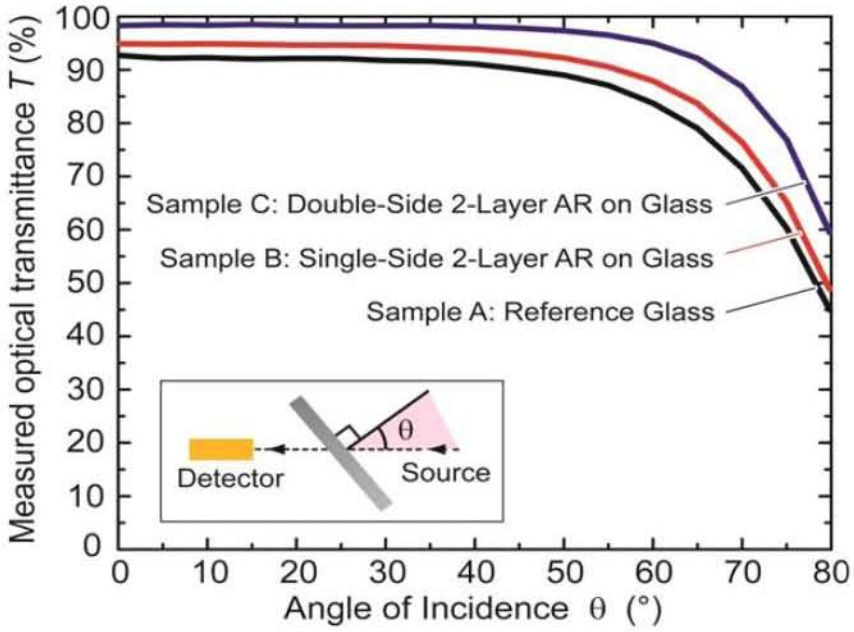

Figure 5.9. Measured angle dependent transmittance of glass substrate with (a) no AR coating, (b) single-side two-layer AR coating, and (c) double-side two-layer AR coating [37].

It shows very-high transmittance over a wide range of incident angles, demonstrating the predicted broadband and omni-directional characteristics of the two-layer graded-index AR coating. The average transmittance, for wavelengths between 350 nm and 1700 nm and incident angles between 0° and 40°, for the uncoated glass substrate is 92% (Sample A) and it increases to 94.6% for glass substrate with two-layer AR coating on one side (Sample B) and further increases to 98.3% for glass substrate with two-layer AR coating on both sides (Sample C).

While the mechanical stability of porous films can be an area of concern, we have not observed any signs of disintegration, degradation of performance, or other adverse effects on these samples even after several months. As a test, we immersed the three samples in an ultrasonic water bath for 15 minutes.

The samples were then blow-dried with N_2 and baked at 120° C for 12 hours in an N_2 ambient. The transmittance of all three samples was then re-measured using the JASCO spectrophotometer; the transmittance showed no significant change at wavelengths longer than 800 nm. The adhesion of the multi-layer AR coating made from nanostructured thin films was tested using a 'scotch tape test' in which a piece of standard adhesive backed packing tape was applied to the sample and then removed. The AR coating was not damaged during the test. The measured average optical transmittance of an uncoated glass substrate between 1000 nm and 2000 nm is improved from 92.6% to 99.3% at normal incidence by using a two-layer AR coating deposited on both surfaces of the glass substrate.

We have also fabricated and tested a number of different step-graded antireflection structures on glass substrates [8, 14, 16, 37–39, 44]. In particular, oblique angle deposition has been used to deposit both two- and three-layer structures comprised of nanostructured SiO_2. These multi-layer antireflection structures have been deposited both on one and on two sides of a glass substrate, and the transmittance characterized as a function of wavelength and incident angle.

Figure 5.10 compares the measured broadband performance of an uncoated glass slide to a glass slide coated on two sides with a multi-layered, nanostructured SiO_2 coating. The nanostructured coatings were prepared in an electron-beam evaporator using different deposition angles to form distinct layers with a step-graded refractive index profile. The inset in Figure 5.10 shows a representative cross-sectional scanning electron micrograph of a two-layer structure. The transmittance of the coated and uncoated glass slides was measured using an angle dependent transmittance measurement setup consisting of a Xenon lamp light source and an Ando AQ6315A optical spectrum analyzer calibrated to detect transmitted photons over a broadband spectrum (400 nm – 1800 nm).

The measured peak broadband transmittance at normal incidence of the uncoated glass slide is 92%, in-line with the expected approximate 4% reflection loss at each glass/air interface. The peak transmittance increases to 98.3% for the double-sided, nanostructured coated glass, implying an average broadband reflection loss of less than 1% at each glass/air interface.

As shown in Figure 5.10, the transmittance through the nanostructured SiO_2 coated glass is also significantly higher than the uncoated glass across a wide range of incident angles. While the transmittance of the uncoated glass slide falls below 80% at an incident angle of 65^o, the glass slide with the double-sided coating still maintains a transmittance above 95%.

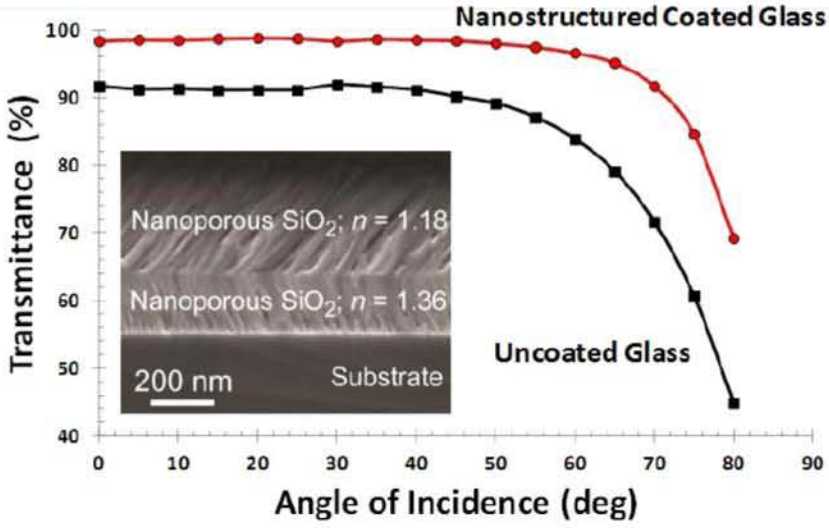

Figure 5.10. Angle-of-incidence dependent broadband transmittance measurement through a glass slide coated on both sides with a step-graded, nanostructured SiO_2 antireflection structure. Also shown is the measured broadband transmittance of an uncoated glass slide, and a cross-sectional scanning electron micrograph of a two-layer nanostructured coating [38].

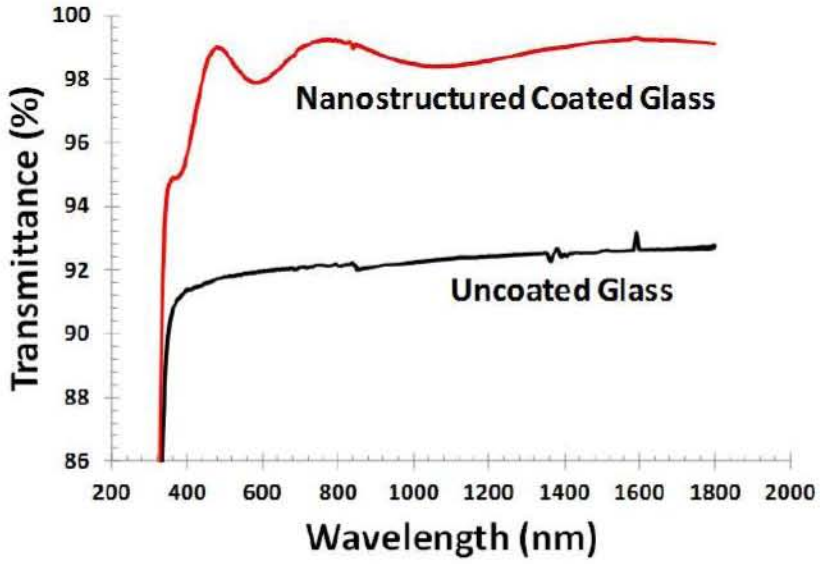

Figure 5.11. Wavelength dependent transmittance measurement of a step-graded, nanostructured SiO_2 antireflection coating on a glass substrate using a JASCO V-570 spectrophotometer [38].

The transmittance of coated and uncoated glass slides has also been measured as a function of wavelength at normal incidence using a JASCO V-570 spectrophotometer.

As seen in Figure 5.11, the measured transmittance through a glass slide is dramatically improved over the entire 400 nm to 1800 nm spectrum by the application of a nanostructured antireflection coating. In particular, the average measured broadband transmittance between 350 nm and 1800 nm increases from 92.2% for the uncoated glass, to 98.6% for the double-

sided, nanostructured coated glass. Moreover, the transmittance through the glass coated with a nanostructured SiO_2 coating exceeds 97.8% at all wavelengths between and 440 nm and 1800 nm, implying a glass-air interface reflectivity below 1.1% over a wide range of wavelengths. Optimized nanostructured antireflection coatings have been shown to outperform an ideal quarter-wavelength MgF_2 coating over all wavelengths and incident angles [14].

We have demonstrated a multi-layer, broadband, Omni-directional AR coating made of a single material with tailored-refractive-index layers on a glass substrate. The availability of the nanostructured low- and tunable-n materials deposited by using oblique-angle deposition has allowed the fabrication of highly effective AR coatings for low index substrates such as glass.

6. Growth of Lab-Scale Nanowire AR Coating

Nanowire AR layers are grown in an electron-beam evaporation system. A fixture modification on the evaporation system allowed demonstrating potential growth on a 3-inch wafer. Figure 6.1 presents the overview of the oblique angle nanowire growth system. The sample is kept at an oblique angle and the crucible that contains the source material or multiple crucibles containing SiO_2 or TiO_2.

Figure 6.1. Thin Film and Oblique angle Nanowire growth Facility.

Figure 6.2 shows the inside view of growth chamber that shows how the sample holder is configured in the growth chamber and the crucible location for the growth of oblique angle nanowire growth. We designed a fixture modification that will allow us to demonstrate potential growth on a 3-inch wafer. Figure 6.2, 6.3 and 6.4 shows the details of the sample holder that is used for growth of oblique angle nanowires. We designed a fixture modification that allowed us to demonstrate potential growth on a 3-inch wafer. Figure 6.5 is an optical photograph of a 3-inch AR-coated glass sample. The substrate is 3-inch diameter N-BK7 glass, a common optical glass used for high-quality optical components. The AR coating consists of a 2-layer step-graded structure of nanostructured SiO_2, similar in design to the one described in Reference [37]. Modified sample mounting procedures were employed to accommodate the larger (and heavier) substrate during the oblique angle deposition.

Figure 6.2. Inside view of the Oblique Angle Nanostructure AR Coating Chamber.

Figure 6.3. Enlarged view of the Nanostructure AR Coating sample holder.

Figure 6.4. Cleaned sample holder and loading of the sample for nanostructure AR- Coating fabrication.

Figure 6.5. Optical photograph of a nanostructured antireflection coating on a 3-inch glass substrate.

7. Large Area AR Coating Development

Large area AR coating has been demonstrated on a 6 inch diameter large substrate, using a larger e-beam evaporation system with high power e-beam gun and thickness monitor. Necessary modifications were made in this system to grow large area AR layers. Figure 7.1 shows the photograph of the electron-beam system used for the growth of large area AR coatings.

Nanostructured AR coatings deposited using the large area AR layer deposition system has the nanostructures similar to the lab-scale samples. Figure 7.2 shows the cross-sectional micrographs of a bi-layer AR layer structure deposited using the large area AR-layer deposition system.

The micrographs in Figure 7.2 show the layers of slanted nano-columns similar to the layer structure observed on lab-scale AR coating. It also demonstrates the controllability of the layer porosity. The bottom layer was grown at a substrate tilt of 54 degree and the top layer was grown at 78 degree resulting two different porosities in these layers.

Figure 7.3 and 7.4 demonstrate growth of oblique angle nanowire AR coatings on 6-inch glass and silicon substrates. The results show that the new larger system is capable of fabricating the nanostructure AR coating on 6-inch substrates. These samples will be characterized in detail and the results will be discussed in future publications.

Figure 7.1. E-beam system with modifications for large area nanostructured anti-reflection layer deposition.

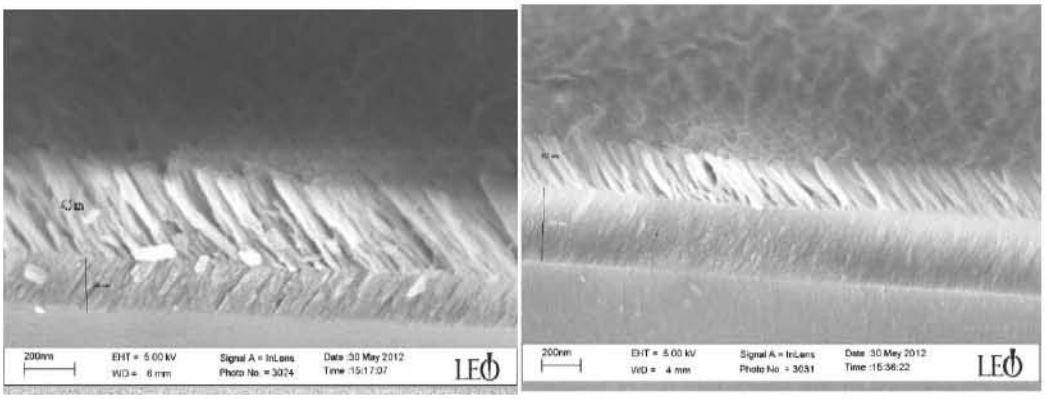

Figure 7.2. Cross-sectional SEM micrographs of a bi-layer AR layer deposited on a 5 inch long silicon substrate. Micrographs were taken on both ends of the sample showing thickness non-uniformity of the layers.

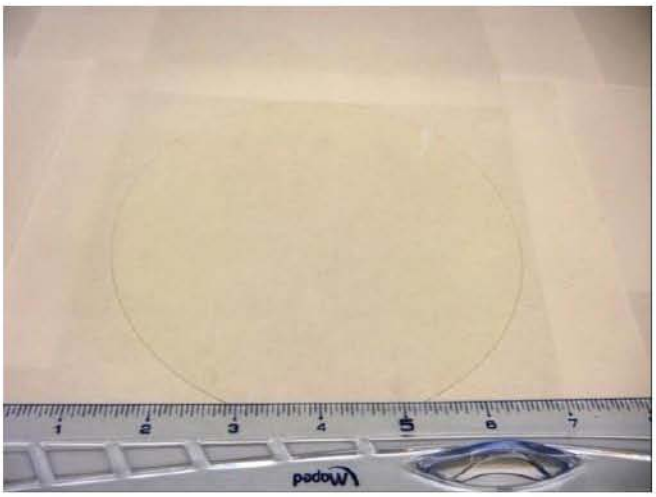

Figure 7.3. Optical photograph of a nanostructured antireflection coating on a 6-inch glass substrate.

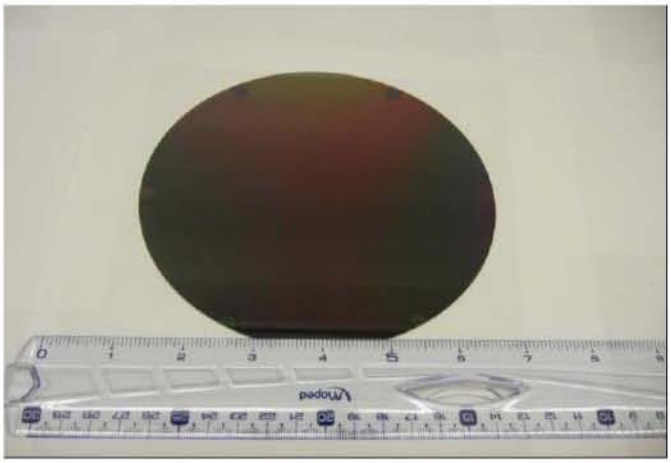

Figure 7.4. Optical photograph of a nanostructured antireflection coating on a 6-inch silicon substrate.

ACKNOWLEDGMENTS

We would also like to acknowledge the support of DARPA for development of the nanostructured AR coating for UV, Visible and IR sensor applications. We would like to acknowledge the support of NYSERDA and the Air Force for its applications for solar cells.

REFERENCES

[1] A. K. Sood, R. A. Richwine, Y. R. Puri, S. Horn, and R. S. Balcerak, "Design considerations using APD detectors for high resolution UV imaging applications," in *Proceedings of the SPIE - The International Society for Optical Engineering*, 2009, vol. 7419, p. (8 pp.).

[2] A. K. Sood, R. A. Richwine, Y. R. Puri, N. DiLello, J. L. Hoyt, T. I. Akinwande, S. Horn, R. S. Balcerak, G. Bulman, R. Venkatasubramanian, A. I. D'Souza, and T. G. Bramhall, "Development of low dark current SiGe-detector arrays for visible-NIR imaging sensor," in *Proceedings of the SPIE - The International Society for Optical Engineering*, 2009, vol. 7298, p. 72983D–72983D–11.

[3] M. Davis, J. W. Devitt, M. E. Greiner, R. Rawe, A. Timlin, and D. R. Wade, "Advanced FPA technology development at CMC Electronics," in *Proceedings of the SPIE - The International Society for Optical Engineering*, 2004, vol. 5563, pp. 62–73.

[4] A. K. Sood, R. Richwine, Y. R. Puri, N. K. Dhar, D. L. Polla, and P. S. Wijewarnasuriya, "Multispectral EO/IR sensor model for evaluating UV, visible, SWIR, MWIR and LWIR system performance," in *Proceedings of the SPIE - The International Society for Optical Engineering*, 2009, vol. 7300, p. 73000H–73000H–12.

[5] P. W. Norton, M. Kohin, M. Dovidio, and B. S. Backer, "Commercialization of uncooled infrared technology," in *Proceedings of the SPIE - The International Society for Optical Engineering*, 2004, vol. 5563, no. 1, pp. 55–61.

[6] A. K. Sood, R. A. Richwine, Y. R. Puri, D. L. Polla, N. K. Dhar, Z. L. Wang, J. M. Xu, P. S. Wijewarnasuriya, N. Goldsman, M. B. Soprano, and B. Lineberry, "EO/IR sensors development using zinc oxide and carbon nanostructures," in *Proceedings of the SPIE - The International Society for Optical Engineering*, 2009, vol. 7318, p. 731804.

[7] A. K. Sood, Y. R. Puri, L. Becker, M. Z. Tidrow, R. S. Balcerak, G. Brill, P. Wijewarnasuriya, N. Dhar, P. Boieriu, C. Fulk, S. Sivananthan, J. Yehoda, and S. Finke, "Development of high-performance radiation-hardened antireflection coatings for LWIR and multicolor IR focal plane arrays," in *Proceedings of the SPIE - The International Society for Optical Engineering*, 2006, vol. 6206, pp. 620613–620615.

[8] XiJ.-Q., M. F. Schubert, J. K. Kim, E. F. Schubert, M. Chen, S.-Y. Lin, LiuW., and S. A., "Optical thin-film materials with low refractive index for broadband elimination of Fresnel reflection," *Nat Phot.*, vol. 1, no. 3, pp. 176–179, Mar. 2007.

[9] J. Zhao and M. A. Green, "Optimized antireflection coatings for high-efficiency silicon solar cells," *Electron Devices, IEEE Transactions on*, vol. 38, no. 8. pp. 1925–1934, 1991.

[10] R. G. Schuhmann and M. Schulz-Grosser, "Multiglass AR coatings in lens designs," 1997, vol. 3133, pp. 256–262.

[11] D. J. Aiken, "High performance anti-reflection coatings for broadband multi-junction solar cells," *Sol. Energy Mater. Sol. Cells*, vol. 64, no. 4, pp. 393–404, Nov. 2000.

[12] B. Kumar, T. Baskara Pandian, E. Sreekiran, and S. Narayanan, "Benefit of dual layer silicon nitride anti-reflection coating," *Photovoltaic Specialists Conference, 2005. Conference Record of the Thirty-first IEEE*. pp. 1205–1208, 2005.

[13] D. J. Poxson, F. W. Mont, M. F. Schubert, J. K. Kim, and E. F. Schubert, "Quantification of porosity and deposition rate of nanoporous films grown by oblique-angle deposition," *Appl. Phys. Lett.*, vol. 93, no. 10, p. 101914, 2008.

[14] R. E. Welser, A. W. Sood, G. G. Pethuraja, A. K. Sood, X. Yan, D. J. Poxson, J. Cho, E. Fred Schubert, and J. L. Harvey, "Broadband nanostructured antireflection coating on glass for photovoltaic applications," *Photovoltaic Specialists Conference (PVSC), 2012 38th IEEE*. pp. 3339–3342, 2012.

[15] G. G. Pethuraja, A. Sood, R. Welser, A. K. Sood, H. Efstathiadis, P. Haldar, and J. L. Harvey, "Large-area nanostructured self-assembled antireflection coatings for

photovoltaic devices," *Photovoltaic Specialists Conference (PVSC), 2013 IEEE 39th.* pp. 99–102, 2013.

[16] R. E. Welser, A. W. Sood, A. K. Sood, D. J. Poxson, S. Chhajed, J. Cho, E. F. Schubert, D. L. Polla, and N. K. Dhar, "Ultra-high transmittance through nanostructure-coated glass for solar cell applications," 2011, vol. 8035, p. 80350X–80350X–7.

[17] Y. Ono, Y. Kimura, Y. Ohta, and N. Nishida, "Antireflection effect in ultrahigh spatial-frequency holographic relief gratings.," *Appl. Opt.*, vol. 26, no. 6, pp. 1142–6, Mar. 1987.

[18] C.-H. Sun, A. Gonzalez, N. C. Linn, P. Jiang, and B. Jiang, "Templated biomimetic multifunctional coatings," *Appl. Phys. Lett.*, vol. 92, no. 5, p. 051107, 2008.

[19] P. B. CLAPHAM and M. C. HUTLEY, "Reduction of Lens Reflexion by the 'Moth Eye' Principle," *Nature*, vol. 244, no. 5414, pp. 281–282, Aug. 1973.

[20] A. Gombert, W. Glaubitt, K. Rose, J. Dreibholz, B. Bläsi, A. Heinzel, D. Sporn, W. Döll, and V. Wittwer, "Subwavelength-structured antireflective surfaces on glass," *Thin Solid Films*, vol. 351, no. 1–2, pp. 73–78, Aug. 1999.

[21] Y. H. Kang, S. S. Oh, Y.-S. Kim, and C.-G. Choi, "Fabrication of antireflection nanostructures by hybrid nano-patterning lithography," *Microelectron. Eng.*, vol. 87, no. 2, pp. 125–128, Feb. 2010.

[22] H. Deniz, T. Khudiyev, F. Buyukserin, and M. Bayindir, "Room temperature large-area nanoimprinting for broadband biomimetic antireflection surfaces," *Appl. Phys. Lett.*, vol. 99, no. 18, p. 183107, 2011.

[23] J. K. Kim, S.-J. Park, S. Kim, H.-H. Park, K. Kim, J.-H. Choi, J. Lee, D.-G. Choi, K. Y. Suh, and J.-H. Jeong, "Fabrication of ZrO2 nanopatterns for biomimetic antireflection by thermal nanoimprint lithography," *Microelectron. Eng.*, vol. 100, pp. 12–15, Dec. 2012.

[24] S.-H. Jeong, J.-K. Kim, B.-S. Kim, S.-H. Shim, and B.-T. Lee, "Characterization of SiO_2 and TiO_2 films prepared using rf magnetron sputtering and their application to anti-reflection coating," *Vacuum*, vol. 76, no. 4, pp. 507–515, Nov. 2004.

[25] R. Prado, G. Beobide, A. Marcaide, J. Goikoetxea, and A. Aranzabe, "Development of multifunctional sol–gel coatings: Anti-reflection coatings with enhanced self-cleaning capacity," *Sol. Energy Mater. Sol. Cells*, vol. 94, no. 6, pp. 1081–1088, Jun. 2010.

[26] H. Nagel, A. Metz, and R. Hezel, "Porous SiO_2 films prepared by remote plasma-enhanced chemical vapour deposition – a novel antireflection coating technology for photovoltaic modules," *Sol. Energy Mater. Sol. Cells*, vol. 65, no. 1–4, pp. 71–77, Jan. 2001.

[27] S. Walheim, E. Schäffer, J. Mlynek, and U. Steiner, "Nanophase-Separated Polymer Films as High-Performance Antireflection Coatings," *Sci.*, vol. 283, no. 5401, pp. 520–522, Jan. 1999.

[28] H. Jiang, K. Yu, and Y. Wang, "Antireflective structures via spin casting of polymer latex," *Opt. Lett.*, vol. 32, no. 5, p. 575, 2007.

[29] H. Selhofer, E. Ritter, and R. Linsbod, "Properties of Titanium Dioxide Films Prepared by Reactive Electron-Beam Evaporation from Various Starting Materials," *Appl. Opt.*, vol. 41, no. 4, p. 756, Feb. 2002.

[30] Y. Zhao, J. Wang, and G. Mao, "Colloidal subwavelength nanostructures for antireflection optical coatings," *Opt. Lett.*, vol. 30, no. 14, p. 1885, Jul. 2005.

[31] M. Kursawe, R. Anselmann, V. Hilarius, and G. Pfaff, "Nano-Particles by Wet Chemical Processing in Commercial Applications," *J. Sol-Gel Sci. Technol.*, vol. 33, no. 1, pp. 71–74, 2005.

[32] B.-T. Liu and W.-D. Yeh, "Antireflective surface fabricated from colloidal silica nanoparticles," *Colloids Surfaces A Physicochem. Eng. Asp.*, vol. 356, no. 1–3, pp. 145–149, Mar. 2010.

[33] A. V Tikhonravov, M. K. Trubetskov, and G. W. Debell, "Application of the needle optimization technique to the design of optical coatings.," *Appl. Opt.*, vol. 35, no. 28, pp. 5493–508, Oct. 1996.

[34] Y.-Y. L. and C.-C. L. and C.-C. K. and W.-C. L. and C.-C. Jaing, "Design of Universal Broadband Visible Antireflection Coating for Commonly Used Glass Substrates," *Jpn. J. Appl. Phys.*, vol. 46, no. 8R, p. 5143, 2007.

[35] M. F. Schubert, F. W. Mont, S. Chhajed, D. J. Poxson, J. K. Kim, and E. F. Schubert, "Design of multilayer antireflection coatings made from co-sputtered and low-refractive-index materials by genetic algorithm," *Opt. Express*, vol. 16, no. 8, p. 5290, Apr. 2008.

[36] N. Yamaguchi, K. Tadanaga, A. Matsuda, T. Minami, and M. Tatsumisago, "Anti-Reflective Coatings of Flowerlike Alumina on Various Glass Substrates by the Sol–Gel Process with the Hot Water Treatment," *J. Sol-Gel Sci. Technol.*, vol. 33, no. 1, pp. 117–120, 2005.

[37] S. Chhajed, D. J. Poxson, X. Yan, J. Cho, E. F. Schubert, R. E. Welser, A. K. Sood, and J. K. Kim, "Nanostructured Multilayer Tailored-Refractive-Index Antireflection Coating for Glass with Broadband and Omnidirectional Characteristics," *Applied Physics Express*, vol. 4, no. 5. p. 052503, 2011.

[38] A. K. Sood, A. W. Sood, R. E. Welser, G. G. Pethuraja, Y. R. Puri, X. Yan, D. J. Poxson, J. Cho, E. F. Schubert, N. K. Dhar, D. L. Polla, P. Haldar, and J. L. Harvey, "Development of Nanostructured Antireflection Coatings for EO/IR Sensor and Solar Cell Applications," *Mater. Sci. Appl. VO - 03*, no. 09, p. 633, 2012.

[39] M. F. Schubert, D. J. Poxson, F. W. Mont, J. K. Kim, and E. F. Schubert, "Performance of Antireflection Coatings Consisting of Multiple Discrete Layers and Comparison with Continuously Graded Antireflection Coatings," *Appl. Phys. Express*, vol. 3, no. 8, p. 082502, Aug. 2010.

[40] D. J. Poxson, M. F. Schubert, F. W. Mont, E. F. Schubert, and J. K. Kim, "Broadband omnidirectional antireflection coatings optimized by genetic algorithm.," *Opt. Lett.*, vol. 34, no. 6, p. 728, Mar. 2009.

[41] S. Chhajed, M. F. Schubert, J. K. Kim, and E. F. Schubert, "Nanostructured multilayer graded-index antireflection coating for Si solar cells with broadband and omnidirectional characteristics.," *Appl. Phys. Lett.*, vol. 93, no. 25, p. 251108, Dec. 2008.

[42] M. Born and E. Wolf, *Principles of optics; electromagnetic theory of propagation, interference, and diffraction of light / by Max Born and Emil Wolf, with contributions by A. B. Bhatia ... [et al.].* Oxford ; New York : Pergamon Press, 1980., 1980.

[43] A. W. Sood, D. J. Poxson, F. W. Mont, S. Chhajed, J. Cho, E. F. Schubert, R. E. Welser, N. K. Dhar, and A. K. Sood, "Experimental and Theoretical Study of the Optical and Electrical Properties of Nanostructured Indium Tin Oxide Fabricated by Oblique-Angle Deposition," *J. Nanosci. Nanotechnol.*, vol. 12, no. 5, pp. 3950–3953.

[44] D. J. Poxson, M.-L. Kuo, F. W. Mont, Y.-S. Kim, X. Yan, R. E. Welser, A. K. Sood, J. Cho, S.-Y. Lin, and E. F. Schubert, "High-performance antireflection coatings utilizing nanoporous layers," *MRS Bull.*, vol. 36, no. 06, pp. 434–438, 2011.